SOFT ROBOTICS
Volume 7, Number 6, 2020

DOI: 10.1089/soro.2019.0090

SoRo
Soft Robotics

ORIGINAL ARTICLE

Continuum Robotic Caterpillar with Wirelessly Powered Shape Memory Alloy Actuators

Colm Mc Caffrey,[1] Takuya Umedachi,[2] Weiwei Jiang,[3] Takuya Sasatani,[3,*] Yoshiaki Narusue,[3] Ryuma Niiyama,[3] and Yoshihiro Kawahara[3]

Abstract

Wireless power transfer (WPT) has the significant potential for soft-bodied continuum robots to extend the operational time limitlessly and reduce weight. However, rigid power receiver coils, widely used in WPT, hinder the continuum deformation of the robot, and as a result, the function realization using the continuum deformation (e.g., locomotion) is impaired. Therefore, this article introduces that a soft-bodied continuum robot can be designed by using thin film receiver coils and an inductively coupled wireless powering solution without sacrificing the continuum deformation and locomotion ability. A system is described for powering and controlling a soft robotic caterpillar consisting of nothing more than its continuum structure, actuators, and thin/flexible power receiving coils.

Keywords: wireless power transfer (WPT), soft-bodied robotics, autonomous mobile robot, shape memory alloy (SMA) coil

Introduction

A POWER SUPPLY is an inevitable issue for an electrically driven soft-bodied *continuum* robot whose body deforms in a complex manner when a roboticist tries to automatize the robot in our daily life or natural environment. It is necessary to feed the power to several actuators independently for a robot to produce complex and adaptive behaviors. Furthermore, in order not to ruin the original softness of the robot, the power source or power receiver must be adequately soft or flexible. Embedding a battery is the most popular method to make the robot autonomous. However, it increases the weight, limits the operating time, and also can stiffen the body.

A significant advantage of continuum robots is that they can utilize the complex mechanical dynamics of the three-dimensional (3D) deformations (e.g., bending, twisting, and buckling) for actuation and sensing purposes.[1–4] This allows the robots to generate versatile motion. However, many of these robots are made autonomous by loading batteries. Incorporating a battery into a robot is severe in that the robot becomes heavy. Furthermore, each time the battery specification (size and dimensions) is changed, it is necessary to redesign the robot design, such as the mass distribution and stiffness distribution. The stiff battery pack can change the robot stiffness distribution, which may ruin the softness of the robot since many electrically driven soft-bodied robots tend to have a small output torque due to the actuators (e.g., shape memory alloys [SMAs][5] and conductive polymer actuators[6,7]). Therefore, a method to feed electricity must be lightweight and flexible not to avoid the inherent 3D deformation of the robots.

Magnetic coupled wireless power transfer (WPT) technology, as described by Shinohara,[8] has a significant potential to alleviate the above-mentioned issues for soft-bodied robots. WPT using resonant inductive coupling was first discovered by Tesla,[9] and a great deal of development[10] has led to an industry worth $1 billion in recent times. One prominent example demonstrated 60 W transmitted over a distance of 2 m at 40% efficiency.[11] In the last decade, WPT research[10,12] encompasses automotive,[13,14] consumer electronics,[15] and charging of implanted devices.[16] WPT to a swarm of robotic devices has been an area of research interest for many years. Devices in the literature are predominantly

[1]VTT Technical Research Centre of Finland, Espoo, Finland.
[2]Faculty of Textile Science and Technology, Shinshu University, Matsumoto, Veda, Japan.
[3]Graduate School of Information Science and Technology, The University of Tokyo, Tokyo, Japan.
*JSPS Research Fellow, Japan.

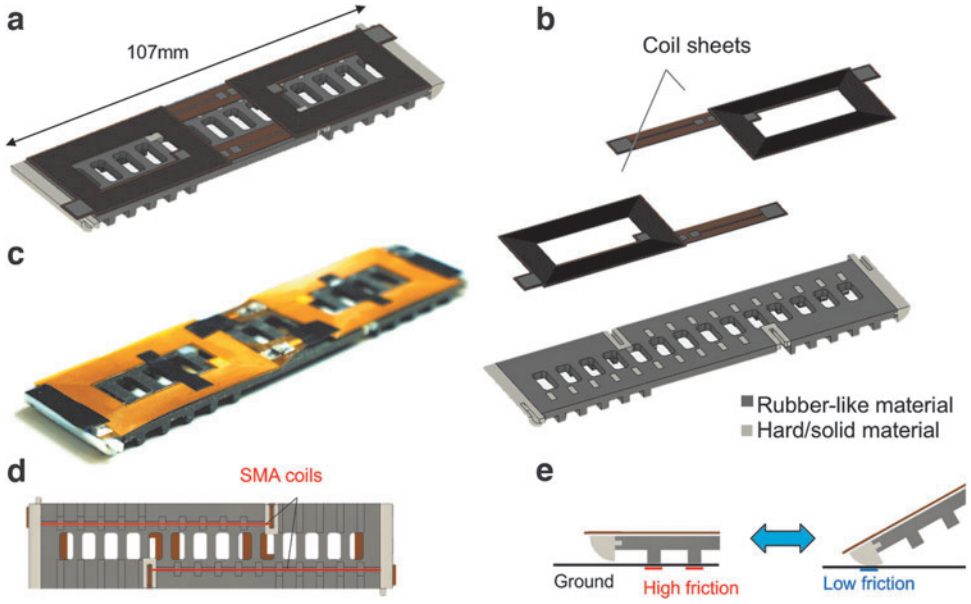

FIG. 1. **(a)** 3D model of the soft robotic caterpillar with wireless power receiver coils assembled. **(b)** Exploded 3D model showing the two receiver coils separately. **(c)** Photograph of the assembled soft robotic caterpillar. **(d)** Model showing the underside of the soft robotic caterpillar and the assembly of the two SMA coils. **(e)** Ground friction switching mechanism. 3D, three-dimensional; SMA, shape memory alloy.

wheel-driven robots with relatively large and rigid wire-wound coils and low transmission frequencies[17] and also include ambulatory insect-type micro-robots.[18] Fully passive systems apply inductive WPT to multichannel shape memory actuators (SMA coils) using frequency multiplexing for actuated origami structure[19,20] and on a micro-scale for micro-fluidic channel actuation,[21] similar to the technique applied in this work. Although the works[19,20] are inspiring, their methods sacrifice the locomotion functionality and designers' degrees of freedom since the methods use rigid coils as the power receivers that stiffen the robot and require some flat rigid surfaces (e.g., a flat origami surface) to attach them. The method cannot be utilized for highly deformable continuum robots that produce locomotion, and therefore, further improvement is needed.

This article presents a caterpillar-like locomotive continuum robot that is powered by WPT technology (Fig. 1). The robot is driven by two SMA coils, which are wirelessly powered and controlled by inductively coupled stimulation from a transmitter coil. As an integral part of the receiver circuit, inductively induced currents are conducted through the SMA coils to generate heat and provide actuation. A planar resonant transmitter coil is designed for uniform magnetic field distribution. A dual *lightweight thin* coil receiver system is designed, which made it possible to attach a thin film feed film to the body of the soft robot without losing the mechanical characteristics of the soft robot. A difference in resonant frequency is applied to each coil to independently actuate the two SMA coil actuators, using a swept frequency stimulus to control locomotion. Particular challenges relate to the powering of a multitude of receiver devices, the changing coupling between transmitter and receiver devices due to the movement, and changing orientation and deformation of receiver coils on the flexible substrate with the movement of the robotic caterpillar. The system delivers powers to two SMA coil receivers at a standoff distance of 20 mm, with an efficiency approaching 30% for each receiver in the coupled system. Forces of 40 g force and 50 g force can be generated in adjacent SMA coils, combined with receiver coils at resonant frequencies of 8.3 and 8.7 MHz. Frequency sweeping at the transmitter coil allows alternate stimulation of SMA coils, giving a wave of force through the robotic caterpillar to generate locomotion of 1.2 mm/s. Advanced control can be performed with more complicated stimulation, including frequency hopping and power modulation. This work represents a significant first step toward wirelessly powered soft-bodied continuum robot swarms.

Proposed Methods

Soft robotic caterpillar

The soft-bodied caterpillar mainly consists of the robot body and two thin, flexible coils. Figure 1a is CAD image of the composite structure, which illustrates the exploded 3D model in Figure 1b. The dark gray and white parts of the body are 3D printed together with a rubber-like material (TangoBlack+; Stratasys Ltd.) and hard/solid material (VeroWhite+; Stratasys Ltd.), respectively, with Objet260 Connex3 (Stratasys Ltd.). The weight of the robot is 7 g, including the receiver coils.

Two SMA coils (Biometal, BMX100; TOKI Corp., Japan.)* are used as actuators. This type of actuators is widely used in soft robotics.[2,5,20,22] The actuators are inserted in the block structures (guides) on the ventral side (Fig. 1d). Inside each black block (Fig. 1d), a block with a hole is printed with the hard/rigid material as a guide for SMA coil, as shown in Figure 1b (the white parts in the beam). The actuators can generate 64 g force by using shape memory effect when it is heated with an input power of 5.4 W/m at a standard drive current of 200 mA. Roughly speaking, SMA can change the stiffness depending on the temperature: high stiffness when it is heated and low stiffness when it is at room temperature. This stiffness change can lead to its contraction when it is extended. The actuator was cut to an original length of 20 mm, extended to about 60 mm, and assembled on the robot. In the extended state at room temperature, the tension

*The coil diameter is 0.4 mm, the wire diameter is 100 μm, and the electric resistance per meter is 900 Ω. The detailed data are available on the following URL: https://www.toki.co.jp/biometal/english/contents.php

of the SMA coil is balanced to the resting state of the flat robot body. When an electric current is conducted through the SMA coil, it causes the heating of the coil, which in turn generates a contraction force. The SMA coil acts to restore the length to the original 20 mm. The actual contraction is not large since the SMA coil is trapped in the rubber beam; however, it is good enough to produce bending motion for the robot locomotion (Fig. 7). This contraction produces bending motion of the part of the soft-bodied continuum beam. When current is removed, the SMA coil cools, leading to a decrease of the stiffness, which in turn makes the robot relax to its flat state (the recovering force stems from the elasticity force of the rubber-like material and the gravity in this experimental arrangement). Activating the contractions of the two SMA coils with appropriate time lag allows the bending wave to transfer from one section of the robot to the another.[22]

The bending motion alternates the friction condition between the ends of the structure. When the structure is flattened, the high friction (black) rubber-like material touches the ground (left in Fig. 1e). However, when the beam part is bending, the high friction material is lifted, and the low friction (white) curved surface touches the ground (right in Fig. 1e). This action allows for the dragging of the low friction element in the contraction phase and eventual restoration of friction in the relaxation phase, which provides forward movement. By generating direct bending waves through controlled actuation of alternate SMA coils, the robot can generate locomotion in either direction.

WPT solution

The inductive coupling between two coils relates to the magnetic fields associated with the current in one coil, which are coupled to and converted to current in another. Without a magnetic core to concentrate the coupling, it can be reasonably presumed that the maximum coupling will be achieved for two identical coils, perfectly aligned with minimum separation between them. Assuming a uniform magnetic field, the coupling is theoretically proportional to the coil's cross-sectional area in the mutual normal plane and inversely proportional to the separation distance. The power transfer efficiency in this study is defined as the ratio of power delivered to the load, to the power output (i.e., the input power including the reflected power) from the source; this refers to the square of linear gain magnitude $|S_{21}|^2$.[15] This efficiency will be dependent most strongly on the resonance frequency matching, the alignment of the magnetic fields, and the impedance matching conditions at both the source and load sides. Actual power transfer refers to the power level delivered to the load, which is maximized for the system that is optimally matched to the source impedance.

The WPT system is based on the near-field resonant inductive coupling between a power transmission coil and two receiver coils, which are directly loaded with SMA coil actuators. Currents are induced in the resonant receiver coils, when conducted in the SMA coil loads generate the heat required for contraction. The system, illustrated in Figure 2a, comprises a vector signal generator for generation of stimulus signals, a linear power amplifier (75 W 50 Ω) connected to our transmission coil. The robotic caterpillar, as previously described, is placed above the transmission coil with the two assembled receiver coils, and SMA coil actuators. The separation distance is kept short in this proof of concept, with a target of 20 mm, which allows transmitter coils to be placed under a table and the caterpillar to crawl on the tabletop.

The system requires to provide the SMA coil actuators with 100 mW (5.4 W/m at the nominal length of 20 mm), with a standard drive current specified as 200 mA. The requirement is

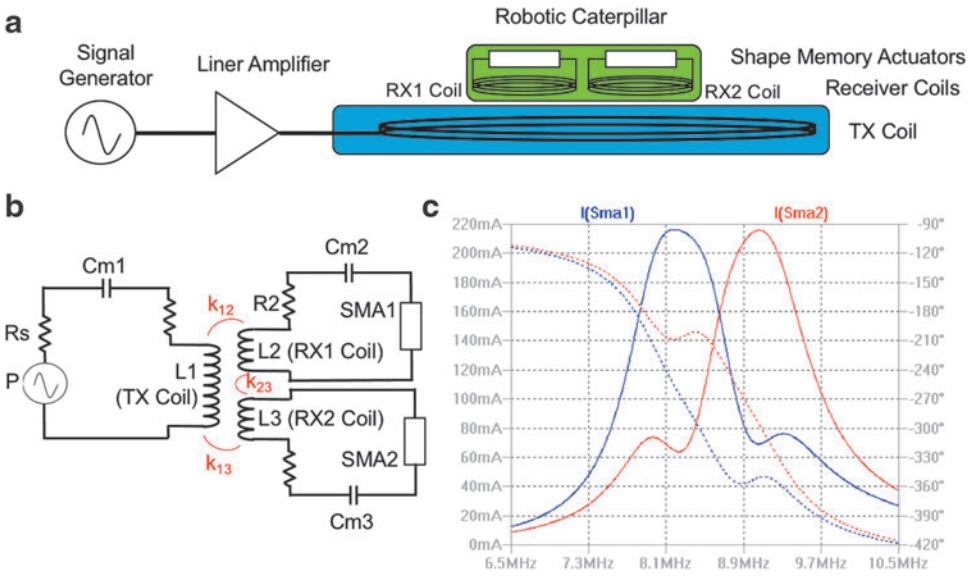

FIG. 2. **(a)** Block diagram of the wireless powering system including R&S® SMBV100A Vector Signal Generator, E&I A-075 Class A Linear Amplifier, transmitter coil platform, and robotic caterpillar with two SMA coils and power receiving coils. **(b)** System schematic with voltage source (P), its series resistance (Rs), transmitter coil L_1 and receiver coils (L_2, L_3) each with series resistance (R_1, R_2, R_3) and resonance tuning capacitors (Cm_1, Cm_2, Cm_3), two SMA coils SMA1 and SMA2, and magnetic coupling coefficients (k_{12}, k_{13}, k_{23}). **(c)** LTSPICE simulation result of the circuit in **(b)** where TX, RX_1, RX_2 are resonant at 8.5, 8.25, and 8.75 MHz, respectively, $P = 20$ V, Rs = 50 Ω, $L_1 = 6.3$ μH, L_2, $L_3 = 12.5$ μH, $Cm_1 = 27.8$ pF, $Cm_2 = 29.8$ pF, $Cm_3 = 26.5$ pF, $R_1 = 3.1$ Ω, R_2, $R_3 = 11.5$ Ω, SMA1 and SMA2 = 25 Ω in series with 145 μH, k_{12}, $k_{13} = 0.1$, $k_{23} = 0.01$.

to allow the possibility to control the actuators independently. The design goal is to maximize power transfer efficiency while trading off the possibility for a broadband transmitter and two small receivers. The aim is maximizing the coupling between the transmitter coil and the two receivers toward the point of critical coupling. When the receivers become over coupled with the transmitter, the peak frequency of power delivery varies due to frequency splitting effects, which consequently results in imprecise power delivery (i.e., the power is not selectively delivered to the intended SMA coil actuators at the intended frequency). In the under coupled case, the power frequency distribution is uniform, but the efficiency is reduced. While maximizing the coupling, attention must be paid to the parasitic parallel capacitance of the coils and related parallel self-resonance frequency. In general, the primary design goal for WPT coils is the optimization for the maximum quality factor, the ratio between the series resistance and inductive reactant at the frequency of interest. In our case, this optimization is also appropriate. The increased inductance will improve coupling to the receiver, whereas the resistance of the coil will directly correlate to the distribution between wasted energy (converted to heat in the coil) to useful energy (converted to heat in the SMA coil).

Transmitter coil. For the sake of simplicity of the aforementioned circuit model, it is beneficial to design a system in which the coupling coefficient between the transmitter and receiver coil maintains a constant value, regardless of the position or configuration of the receiver coil. This is essential in the proposed caterpillar system since the receiver side is fully passive (utilizes no power management units), and therefore, the input power needs to be controlled at the transmitting side. For maintaining this approximation, the fluctuation of the coupling coefficient between the transmitter and receiver coil is targeted to be kept as small as possible. The receiver coil is a simple multi-turn spiral coil, and the operation range of the WPT caterpillar in this study is within a planer surface. Considering these conditions generating an approximately uniform magnetic field by the transmitter coil within the operation range presents a practical solution for maintaining approximately constant coupling coefficient.

The simplified schematic of the system is given in Figure 2b. The schematic neglects the parallel capacitance between adjacent turns of the coils as well as the capacitive coupling between coils. These parasitic impacts are minimized through design, as described in the following sections. The power amplifier is represented as a 50 Ω voltage source. The transmission coil is described with the inductor L_1, and it is series resistance R_1 at the transmission frequency. A high voltage, low equivalent series resistance, the capacitor is included to tune the coil to series resonance at 8.5 MHz. On the receiver side, the two coils are modeled similarly with inductors L_2 and L_3 and series resistances R_2 and R_3. These coils are tuned to series resonance at 8.25 and 8.75 MHz, respectively, with series capacitors Cm_2 and Cm_3. The magnetic coupling coefficient between the transmitter and receiver coils is given as k_{12} and k_{13}, whereas coupling between adjacent receiver coils is represented by k_{23}.

The circuit, as shown in Figure 2b, with the coils' parasitic parallel capacitances, was simulated in LTSPICE with a sweeping input frequency from 6.5 to 10.5 MHz. The circuit simulation was used to find suitable resonance frequencies of the two receiver coils and to evaluate the target optimal coupling coefficient between the transmitter and receiver, the maximum tolerable coupling between adjacent coils, and the impact of other factors including the coils series resistance, inductance, and the source resistance. While the simulation was used for the optimization of the target parameters, the circuit elements shown in Table 1 represents the measured parameters of the coils from the implemented system. For a 20 V input, a maximum current just under 220 mA is coupled to the receivers when a coupling coefficient of 0.1 is applied. The frequencies of maximum current deviate slightly from the receiver resonances to 8.15 and 8.88 MHz, due to the minor, but tolerable frequency splitting. At the frequency where the maximum current is coupled to one coil, a current of ~80 mA is coupled to the other. As this is 20% of the 200 mA required drive current, it should not affect the SMA coil state of contraction, so it is tolerated for the application.

Table 1. Comparison of Simulated and Measured Parameter of the Transmitter Coil at 8.5 MHz

	Simulated	*Measured*
Impedance	2 + j365	3.1 + j353
Q factor (X/R)	183	114
Series resonance cap, pF	51.3	51.5
Self resonance (parallel), MHz	28.6	21.1

Generally, if a planar spiral coil is wound with uniform distribution, the magnetic field in the center of the coil would be much more intense than near the edges of the coil. Therefore, using dense turns at the edges of the coil and making the turn sparse distribute further toward the center of the coil is a frequently used method to achieve uniform magnetic field distribution. Many studies propose to adjust the density of these turns using exhaustive parameter sweeps[23] and intuition,[24] which can be adopted in arbitrary spiral coils, and solving inverse problems described as below, which can only be used in a circular spiral coil.[25] Within these methods, this work adopts the latter method that solves the inverse problem. For the sake of simplicity, the coil shape is selected to be a circular spiral coil; this brings about an axial symmetry, which simplifies the coil design process.[25] The method which solves the inverse problem considers the distribution of the magnetic field as a linear transformation of the distribution of current, therefore the density of turns. The inverse matrix of the linear transformation of current distribution then represents the magnetic field distribution.

The transmitter coil was designed to have a diameter of 150 mm and five turns. Applying the design method described above, the appropriate radii of respective turns can be calculated according to the formula given in the following equation:

$$\frac{r(i)}{R_{\text{out}}} = \frac{1 - \exp\frac{-\frac{i}{N}}{\delta_w}}{1 - \exp\frac{-1}{\delta_w}}. \quad (1)$$

The above equation is based on the design of the transmitter coil proposed by Waffenschmidt.[25] N and $r(i)$ are the number of turns and the trace position of the turn with index i, whereas R_{out} and δ_w are the outer radius and the fit parameter optimized in the study of Waffenschmidt.[25] The designed

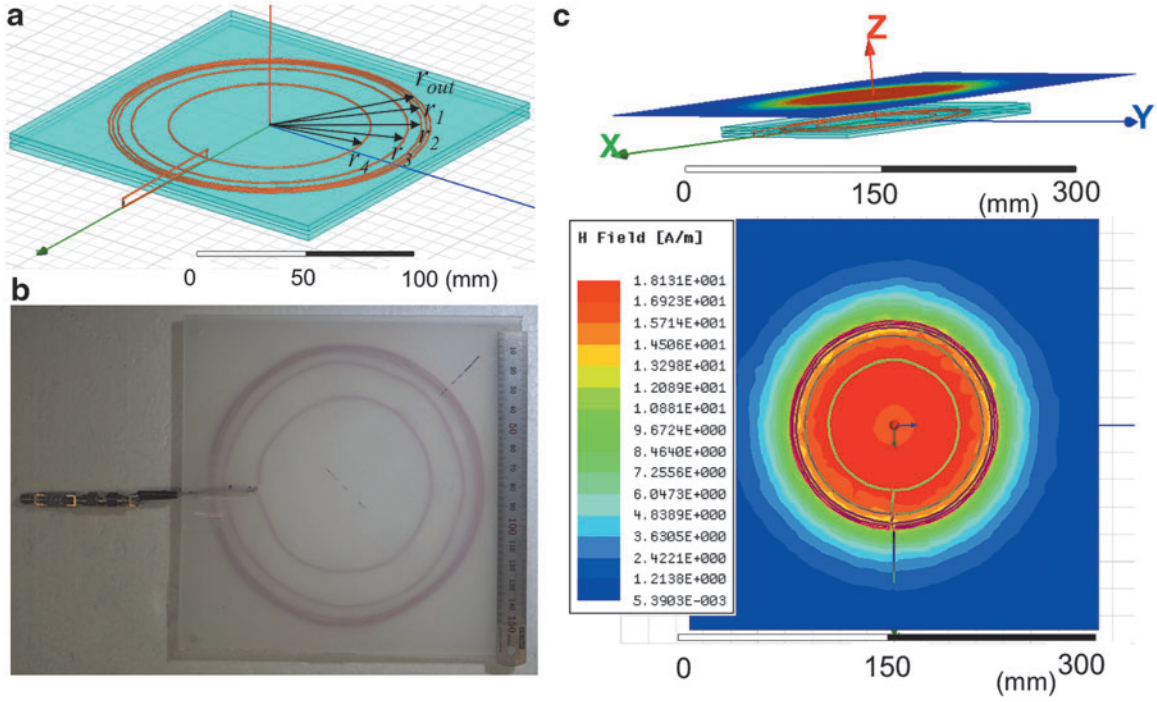

FIG. 3. **(a)** 3D model of the transmitter coil in Ansys HFSS. **(b)** Assembled transmitter coil with resonance tuning capacitor and Subminiature-A connection. **(c)** Magnetic field distribution simulations at 10 mm distance from the coil. HFSS, high-frequency structure simulator.

coil was simulated in Ansys high-frequency structure simulator (HFSS) with a 4 mm thick polyethylene plastic layer above and below with dielectric constant of relative permittivity (or ε_r) and loss tangent (or tan δ). The simulated transmitter coil gave an impedance of $2+j\times365$ at 8.5 MHz, corresponding to a quality factor of 183, and came to parallel resonance at 28.6 MHz. The coil was matched to resonance by connecting a series capacitor of 51.3 pF. The magnetic field at 8.5 MHz was examined at a distance of 10 mm from the top polyethylene layer; this is considered as the typical height of our receiver coils on the robot. The magnetic field distribution illustrated in Figure 3c shows that the intensity of the magnetic field is more than 81% of the peak value within the coil radius; this intends that the designed transmitter coil is generating a magnetic field with nearly uniform field intensity. The coil was fabricated, Figure 3b, using litz copper wire (660/46) in between two 4 mm sheets of polyethylene plastic with a small printed circuit board for matching capacitance and Subminiature-A coaxial connector to interface the power amplifier. The unmatched coil was measured to extract the inductive part of its impedance, and the resistive element was measured with a 51.5 pF series capacitance. The measured impedance of $3.1+j\times353$ represents an increase in resistance used over the simulated coil, while the inductance is slightly reduced in the measured coil. The differences are most likely due to the inaccuracy in the resistivity of the assumed perfect copper wire in the simulation and underestimate of the losses in the polyethylene plastic, at the interconnection points and in the capacitor.

Receiver coil. For the wireless power receiver, the requirements of the device would be (1) to receive maximum power from the incident magnetic field, (2) to provide maximum power transfer efficiency to the SMA coil load, and (3) to minimize the effects of cross-coupling to nearby receivers. In considering maximum power, the fundamental relationship relates to the mutual coupling between transmitter and receiver. This relates to the transmitter's magnetic flux, which intersects the conductors of the receiver coil, represented by the mutual inductance. Therefore, the effective surface area in the plane of incident magnetic flux can be considered to be the dominant contributor along with receiver coil inductance. For power transfer efficiency, the power losses throughout the whole system must be considered. In respect to the receiver coil, the dominant aspect in the losses relates to the series resistance presented by the coil conductors. It is clear from Figure 2b that any power delivered to the receiver will be divided between the coils' series resistance and the SMA coil itself. The coil in Figure 2b is manufactured by a company called P-ban.com. The double-layered polyimide substrate's thickness is 25 μm, and the conductor is etched copper.

The coils' external dimensions were dictated by the dimensions of the caterpillar itself and the placement of the SMA coil actuators. The maximum width of the receiver coils was applied as 25 mm the same as the caterpillar's width, and 40 mm was selected for the length. Therefore, 80% of the caterpillar's surface area would be covered by the power receiving coils with a lateral separation gap of 20 mm; this gap was inserted to ensure that the coupling between adjacent receiver coils was insignificant in comparison to the coupling between the receiver and the transmitter coil. Therefore, the primary parameters for optimization are the coil's self-inductance, for maximization of coupling, and the coils series resistance for maximization of power transfer efficiency to the load. The maximization of the receiver coils quality

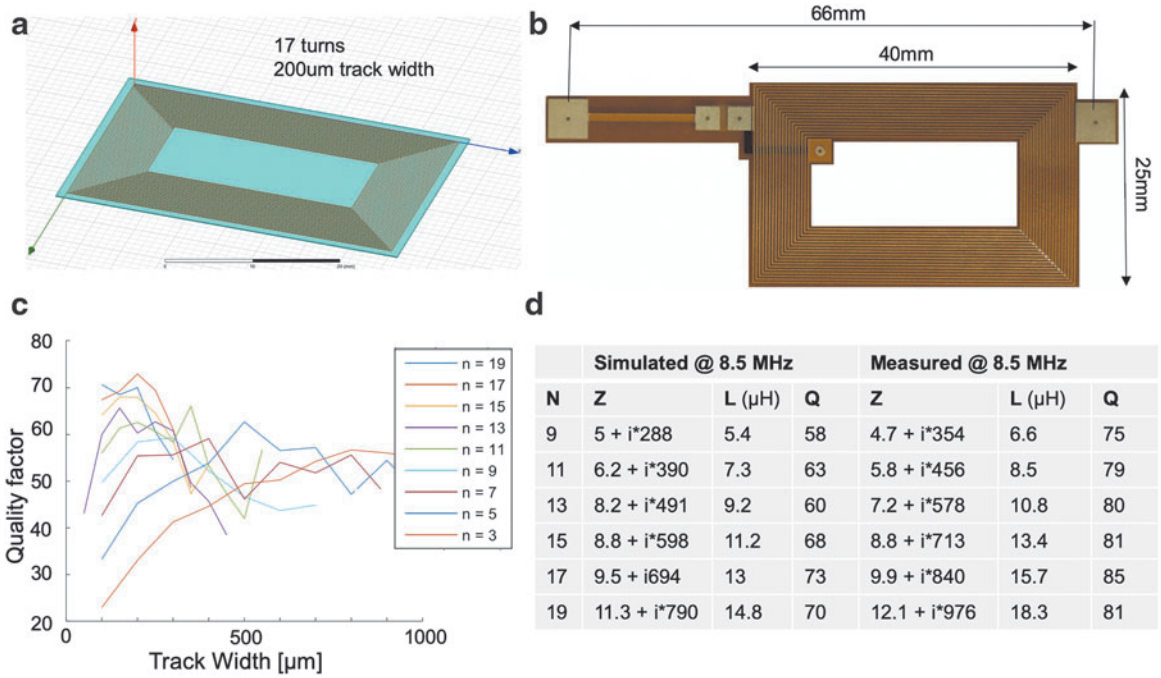

	Simulated @ 8.5 MHz			Measured @ 8.5 MHz		
N	Z	L (μH)	Q	Z	L (μH)	Q
9	5 + i*288	5.4	58	4.7 + i*354	6.6	75
11	6.2 + i*390	7.3	63	5.8 + i*456	8.5	79
13	8.2 + i*491	9.2	60	7.2 + i*578	10.8	80
15	8.8 + i*598	11.2	68	8.8 + i*713	13.4	81
17	9.5 + i694	13	73	9.9 + i*840	15.7	85
19	11.3 + i*790	14.8	70	12.1 + i*976	18.3	81

FIG. 4. **(a)** 3D model of the coil for optimization in Ansys HFSS. The example has 17 turns and a track width of 200 μm. **(b)** Photo of the fabricated example coil on polyimide flex substrate. **(c)** Results of the Ansys HFSS simulations, showing quality factor optimum for the example coil. **(d)** Comparison of the simulated and measured parameter of the receiver coil at 8.5 MHz.

factor, defined as the ratio between the coils inductive impedance and series resistance at the target frequency, 8.5 MHz, was applied as the optimization target with the number of turns and conductor track width and spacing as the optimization parameters.

The core of a single receiver coil is illustrated in Figure 4a. For the optimization, the external dimensions are fixed at 40×25 mm while the number of turns was increased from 3 to 19 and the width of the conductor was increased from 100 to 1000 μm to the extent that the fixed area would allow. The coil was simulated on a 38 μm polyimide substrate, between 1 and 10 MHz in free space, using Ansys HFSS. The inductance and series resistance were extracted for each coil, and the quality factor at 8.5 MHz was calculated in each case. The results, shown in Figure 4c, demonstrate an optimum emerging for a coil with 17 turns and a track thickness of 200 μm. Indeed, there was a tendency of coil's with various turns toward optimal quality factor for a track thickness of 200 μm, so six coils with 9–19 turns were fabricated and tested for comparison. The fabricated coil of 17 turns and 200 μm track thickness is photographed in Figure 4b and a table of the fabricated coils simulated impedance, and quality factor is shown in Figure 4d. The coil measurements were conducted using an R&S® Vector Network Analyzer to measure impedance at 8.5 MHz. The inductance of each coil was measured from the imaginary part of input impedance with the coil alone. As for the copper loss (i.e., the real part of input impedance), naively extracting the real part of impedance results to a large error; this is because the imaginary part of the input impedance is much larger than the real part for high-Q coils. To enable accurate measurement, the coils were first tuned to series resonance (i.e., the imaginary input impedance is near zero) at 8.5 MHz using low loss capacitors and the real impedance was measured in this condition; this suppresses the imaginary part of impedance and enables rather accurate measurement of the real part with a vector network analyzer. The quality factor was then calculated using the well-known standard equation for series resonance circuits ($Q = \omega L/R$, at 8.5 MHz).[26] There are notable differences between the simulated and measured values of impedance. Up to 20% more inductance was measured, which can be attributed to additional tracks and interconnects on the measured loop compared to the simulated one and the dielectric constant of the polyimide, quoted with a large range of error (3–3.8 for DuPont Kapton) depending on relative humidity. The measured losses (real impedance) were slightly less for lesser turn coils and slightly more for higher turn coils, with a maximum difference of 7% attributed to the compounding effects of the additional conductors and the dielectric losses of the polyimide substrate, which were quoted with a large range of error (0.0015–0.0035 for DuPont Kapton) depending on relative humidity. Since the differences are systematic, and the optimization pattern clearly correlates, the measurements were considered a satisfactory verification of the optimization.

Experiments

The following experiments were conducted with the transmitter coil described in Figure 3, whose results are indicated in Table 1. The optimized receiver with 17 turns, 200 μm (described in Figure 4) is chosen based on the results shown in Figure 4d. Three receiver coils were tested. So that power could be controlled by transmission frequency sweeps,

the receivers used in the robot had to be separated in resonance frequency, and therefore were tuned to resonance at 8.31 and 8.71 MHz. A reference receiver coil was included in the tests, which had matched resonance frequency to the transmitter loop (at 8.58 MHz).

Coupling, power efficiency, and power transfer

The mutual inductance between two coils can be estimated by measuring the difference in their series-connected inductance when coupled and uncoupled. The coupling coefficient can be evaluated as the mutual inductance divided by the square root of the product of individual inductance. The mutual coupling was measured for the unmatched series-connected coils in three cases: (1) the receiver in the uncoupled condition is removed from the transmitter field, (2) the receiver in closely coupled condition is in the center of the transmitter loop and on the polyethylene surface, and (3) in lightly coupled condition. The receiver is placed in the center of the transmitter loop radius and 20 mm from the polyethylene surface. Experiments were conducted on the 17 turn, 200 μm, 15.7 μH receiver coil (Fig. 4) and the 6.6 μH transmitter coil (Fig. 3) and mutual inductance values of 1.5 and 0.9 μH were measured (corresponding to coupling coefficients of 0.15 and 0.09) for closely coupled and lightly coupled coils, respectively.

The power transfer efficiency was measured by connecting the transmitter and two receivers (including both receiver coils without SMA coil actuator) to Port 1, 2, and 3, respectively, of an R&S Vector Network Analyzer and examining the scattering parameter S_{21}/S_{31} (power transfer efficiency = the square of S_{21}/S_{31}). Note that the impedance of the SMA coil varies with length and temperature; therefore, it is difficult to evaluate the actual efficiency through measurements. To obtain the approximate efficiency, we conducted measurements using 50 Ω instruments. The power transfer efficiency was evaluated when the resonance frequency of the receiver was offset from that of the transmitter as required to control independently multiple SMA coils. Receivers resonating at 8.31 and 8.71 MHz were selected as a good compromise between efficiency and frequency separation with a transmitter coil matched at 8.58 MHz, resulting 34% and 37% power transfer efficiencies, respectively. The low levels of efficiency observed are predominately due to the resonant frequency mismatch between the transmitter and receiver coils, as was necessary to control power delivery by frequency sweeping. Also, impedance mismatch on both the transmitter and receiver coils, along with restive losses in these coils reduce the efficiency.

The system for wirelessly powering and controlling the caterpillar was constructed, as illustrated in Figure 5a. An R&S® SMBV100A Vector Signal Generator was used for a signal generation; power amplification was provided with an E&I A-075 Class A Linear Amplifier with 50 Ω output impedance. An AR DC3401 bidirectional coupler was placed between the amplifier and the transmitter loop, and R&S® NRP-Z91 power measurement devices were used to measure the forward power (i.e., the total power input) and reflected power (i.e., the power loss due to the impedance mismatch at

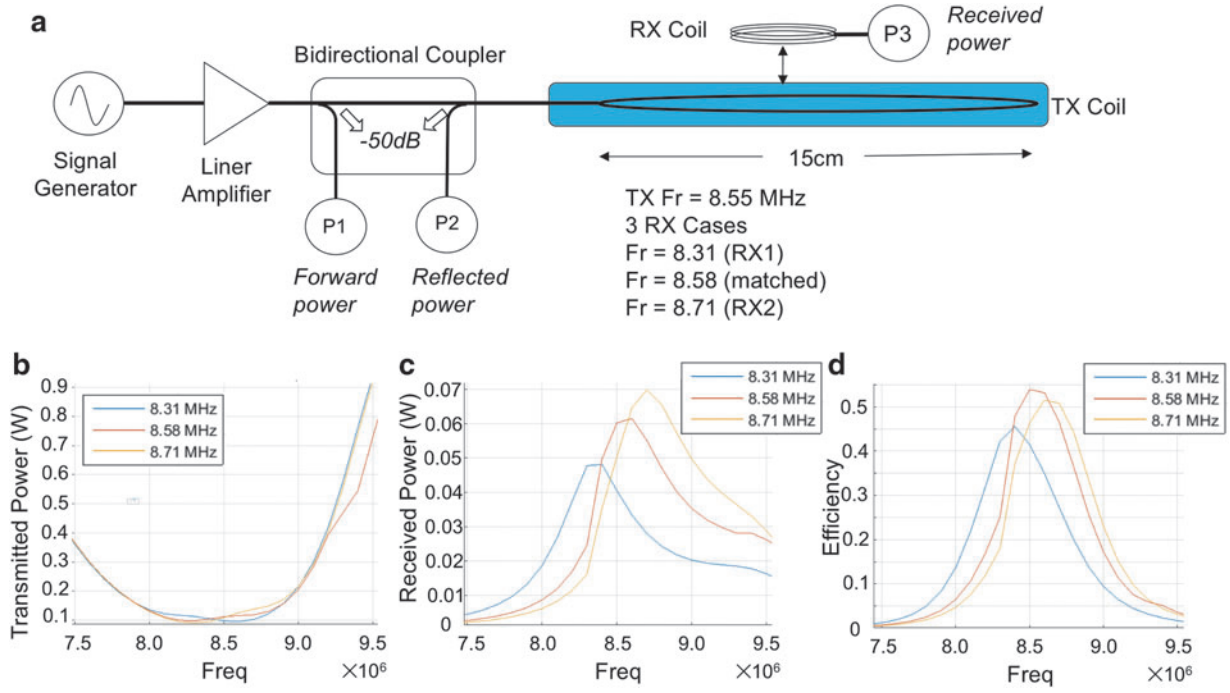

FIG. 5. **(a)** System for power transfer measurements including R&S SMBV100A Vector Signal Generator, E&I A-075 Class A Linear Amplifier, AR DC3401 bidirectional coupler, R&S® NRP-Z91 power measurement devices P1, P2, P3, transmitter coil and receiver coil with 17 turns and track width of 200 μm. **(b)** Measured transmitted power for three receiver coils resonant frequencies of 8.31, 8.58, and 8.71 MHz. **(c)** Measured transmitted power for the three receiver coils. **(d)** Efficiency (received/transmitted power) for the three receiver coils. Signal generator outputs a power level of −10 dBm in all cases **(b–d)**.

the source) levels. The receiver coil was placed in the center of the transmitter loop at a separation distance of 20 mm with a third R&S NRP-Z91 power measurement device to measure the transmitted power (i.e., the power delivered to the load). The signal generator, outputting −10 dBm (0.1 mW delivered to the 50 Ω amplifier), stepped the output frequency from 7.5 to 9.5 MHz in steps of 100 kHz. The measured power delivered to the transmitter loop is plotted in Figure 5b. The power levels in this experiment are significantly lower than those needed to power the SMA coil, but the linear nature of the system allows direct scalability. While the signal generator outputs a constant 0.1 mW, the power delivered to the transmitter loop depends on the impedance seen at the amplifier output. At resonance, the power amplifier sees a purely resistive load, and the power delivered is a minimum while outside resonance larger powers are delivered and reflected by the mismatched system, reaching 380 mW at 7.5 MHz and 900 mW at 9.5 MHz. The real power delivered to the three receiver coils (measured separately) is shown in Figure 5c, whereas the efficiency is shown in Figure 5d. The maximum powers received were 48, 62, and 70 mW for the receiver coils matched at 8.31, 8.58, and 8.71 MHz.

Mechanical characterization

As a preliminary experiment before locomotion experiment, force measurement experiment of SMA and posture analysis of the caterpillar robot are conducted (Fig. 6a, b, respectively). Force measurement of the wirelessly powered SMA coils was conducted with an experiment setup described in Figure 6a. An SMA coil attached with the optimized receiver coil (without the robot body) was placed over the transmitter coil with a separation distance of 20 mm. One side of the SMA coil was fixed to a rigid frame, whereas the other was attached to the force measurement device (Force gauge; Shimpo FGP-0.5, Japan). The force measurements were carried out with receiver coils resonant at 8.31, 8.55, and 8.71 MHz. Figure 6b shows the experiment results. The force generated by the receiver coils correlates well with the measurement of real power delivered in Figure 5. Examining the result of Figure 6b, with attention to the selected receivers (resonant at 8.31 and 8.71 MHz), it is clear that we can independently control the two SMA coils by transmitting power at different frequencies and that a controlled wave of force can be propagated through the caterpillar by sweeping the transmitted frequency.

The complete wirelessly powered caterpillar (Fig. 1) was assembled, with the selected 8.31 and 8.71 MHz coils used to power the SMA coils, as illustrated in Figure 1d. The caterpillar was placed in the whole wireless power system consisting of the signal generator, linear amplifier, and transmitter coil shown in Figure 2a, with a separation distance of 20 mm. A preliminary test was performed to confirm that the proposed system was capable of activating the SMA coils selectively in a manner appropriate to control the posture, and therefore the locomotion, of the caterpillar. The signal generator, outputting 0 dBm (1 mW), stepped the frequency every 2 s from 7.8 to 9.2 MHz in increments of 200 kHz. Figure 6c shows snapshots of the experiment, which indicates that the curvature peak gradually shifted from the

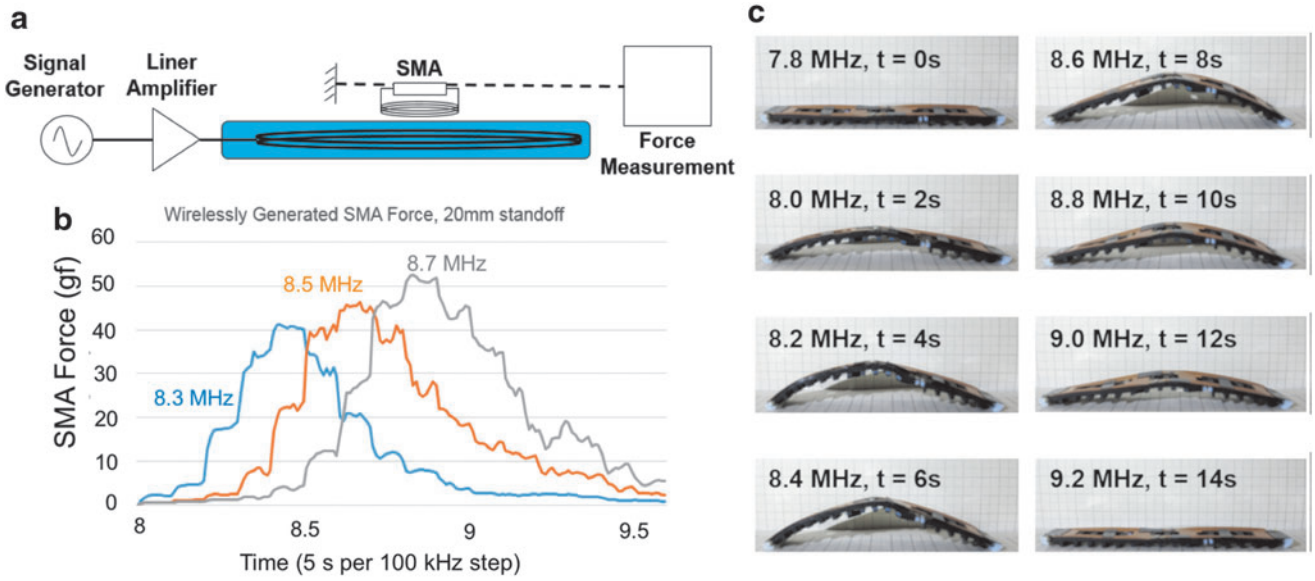

FIG. 6. **(a)** System setup for the characterization of the force generation of the wirelessly powered SMA coil receiver including R&S SMBV100A Vector Signal Generator, E&I A-075 Class A Linear Amplifier, transmitter coil resonant at 8.55 MHz, receiver coils resonant at 8.31, 8.58, and 8.71 MHz at a separation distance of 20 mm, and force measured with Shimpo FGP-0.5. **(b)** Results of the force measurement setup of **(a)** with frequency increments of 100 kHz at 5 s intervals, and approximate coil resonant frequencies shown with each curve (same color). **(c)** Analysis of the caterpillar posture at frequencies from 7.8 to 9.2 MHz in increments of 200 kHz at intervals of 2 s. The both SMAs are totally relaxed ($t = 0$–2 s, State 1). SMA1 (*left*) is reaching max heating around the frequency sweeps near to 8.31 MHz ($t = 4$–8 s, State 2). SMA1 is less heating, whereas SMA2 is heating when the frequency sweep is near to 8.5 MHz ($t = 8$–10, State 3). When the sweep is near to 8.7 MHz, SMA1 is less heating, SMA2 is reaching max heating ($t = 10$–12 s, State 4). When the sweep to the end, SMA1 and SMA2 are relaxing ($t = 12$–16 s, State 5).

left (8.2 MHz, $t = 6$ s) to the right (8.6 MHz, $t = 12$ s), as the two SMA coils are separately actuated.

Locomotion with frequency sweeps

Frequency sweeps are utilized to control the wireless power to the SMA coil receivers consecutively for achieving locomotion. The same frequency range (7.5–9.5 MHz) was swept in increments of 100 kHz and a 100 ms dwell time, which were generated from a Vector Signal Generator (R&S SMBV100A) remotely controlled via an IEEE-488 GPIB interface. The signal generator, outputting 4 dBm (2.5 mW), with the increased power needed to actuate the SMA coils in a faster sweep than that shown in the Mechanical Characterization section. In between sweeps, 1 s interval time allows the cooling and therefore ''relaxing'' of the SMA coil actuators.

The experiment result is demonstrated in Figure 7. An integral round of frequency sweeps resulted in five states of the soft-robotic caterpillar. (1) At the initial state, when the frequency starts sweeping at 7.5 MHz, negligible power is delivered to both SMA coil receivers, the soft-robotic caterpillar is flat and inactive. (2) At the second state, when the frequency sweeps to 8.3 MHz, the front SMA coil receiver heats up with increasing wirelessly transmitted power due to inductive resonance, whereas the other SMA coil receiver remains in the inactive state, which causes the rear part of the soft robotic caterpillar to bend. (3) In the third state, when the frequency sweeps to 8.5 MHz, the wirelessly transmitted power to the rear SMA coil receiver decreases, whereas the other SMA coil receiver, with resonance frequency at 8.7 MHz, acquires more wireless power, starting generating a bending wave for locomotion. (4) At the fourth state, when the frequency sweeps to 8.7 MHz, the rear SMA coil receiver starts relaxing with less wirelessly transmitted power, whereas the other SMA coil receiver reaches its maximal heating state, with the bending wave propagating to the front end of the soft-robotic caterpillar. (5) At the final state, when the frequency sweeps to 9.5 MHz, both SMA coil receivers relax, the soft-robotic caterpillar returns to be flattened. This completes the cycle of locomotion, and after 1 s relaxing time, the next cycle begins. The technique can work to move the caterpillar in either direction by reversing the direction of the frequency sweep. One cycle of the locomotion described here is illustrated in Figure 7a, and a plot of the distance traveled of the robots front and back legs for 28 s is plotted in Figure 7b. From these results, the forward motion of the robot is at a rate of 7.5 cm/min.

Conclusion and Further Work

The work has demonstrated a wirelessly actuated soft-bodied caterpillar-based locomotive robot. Shape memory actuators were combined with a near-field resonant inductive WPT system for powering and control of the robotic caterpillar's movement. The developed system delivered sufficient power to the two SMA coils at efficiencies of $\sim 30\%$ with a separation of 20 mm between transmitter and receiver in the proof of concept. Two SMA coils were independently controlled using a wide bandwidth transmission system with 50 Ω power amplifier and SMA coil receiver coil combinations set to series resonance at different frequencies. A simple linear frequency sweep was shown to create a wave of force through the robotic caterpillar, such as to generate forward locomotion at a rate of 7.5 cm/min.

The wireless power system developed in this work is not without its limitations, and there are significant challenges to address in future work. A fundamental limitation relates to the separation distance between the transmitter and receiver coils. The system was optimized at 20 mm, for demonstration of the concept with transmitter coil under a table and the caterpillar crawling on the tabletop. Experimentation suggested that SMA coil actuation was possible at separation distances close to 200 mm at the cost of much-reduced efficiency and corresponding higher powers to be transmitted. Incremental improvements in the design may bring a slight reduction in losses and, therefore, in increases in range, however, fundamental limitations on inductively coupling power to a small receiver coil limit range to the order of

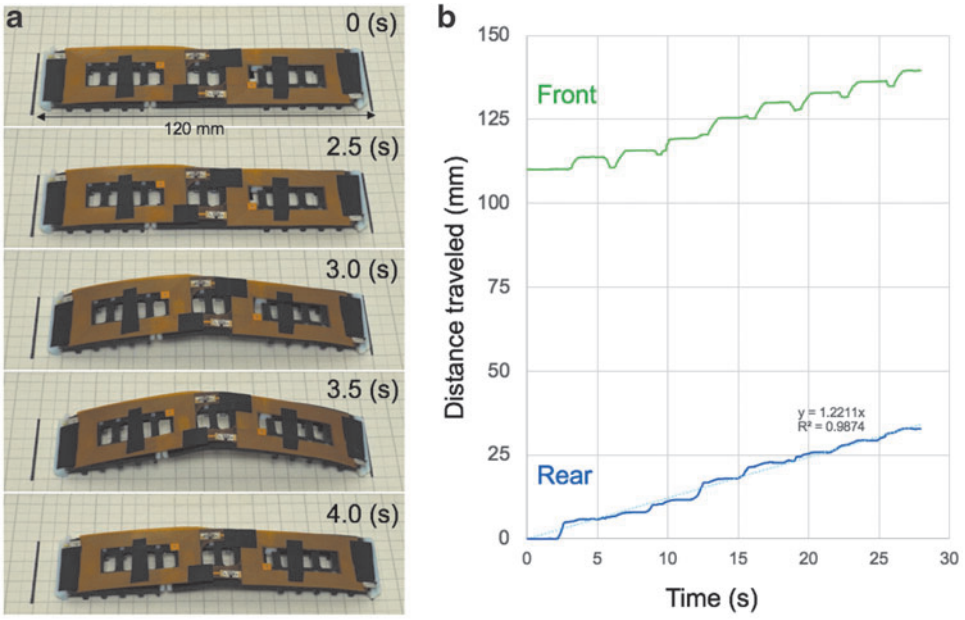

FIG. 7. **(a)** One sequence of the crawling locomotion of the robot. **(b)** The trajectories of the front and rear legs of the robot for 28 s.

100 mm, as is the case in all near field powering systems. Far-field WPT using beam focusing and steering could enable ranges in the order of meters, which would enhance the usefulness of the device in real applications.

The dimensions of the transmission coil were kept small for the proof of concept demonstration, which implies a restriction in the accessible area for the robot. The transmitter coil could be scaled, but it would be limited, at approximately double the diameter, by the self-resonance behavior and the power available from the amplifier. An alternative method for scaling would be to make an array of transmitter coils as in the study of Waffenschmidt,[25] or applying an array of individual coils and intelligent multi-hop algorithm to activate those closest to the caterpillar. Another fundamental limitation relates to the impedance variation of the whole system seen at the power amplifier. The system is tuned to a specific operating condition. Changes in the environment, such as foreign metallic objects, might cause detuning of the system, such as to reduce the efficiency drastically or prevent the correct operation of the device. A more optimized system will provide impedance measurement of the transmitter loop and apply smart control algorithms to regulate the transmitted power levels. These challenges reflect typical opportunities for future developments in the field of WPT.

The locomotion control system presented here focused on the application, which required two independently controlled SMA coil actuators. More advanced soft robotic applications can be enabled by increasing the number of actuators. For example, a soft robotic caterpillar driven by three SMA coils can provide not only forward and reverse locomotion but also steering control. Expanding further the number of receivers, such as to use multiple robots, presents a very challenging development. The actuator control algorithms here developed were rather primitive, based on linear frequency sweeps. The research will continue on more advanced control enabled by various frequency switching methods and power modulation techniques. Furthermore, the slow rate of locomotion demonstrated in this work was related to natural caterpillar locomotion rates and limited also be the simplistic frequency sweeps. Further research into the various techniques of pulsed and sweeping power transmission can significantly accelerate the caterpillar locomotion.

This wireless power supply system will be a handy tool for researchers and engineers who develop autonomously driven soft-bodied robots. Because the receiver coil(s) can be attached on a deformable surface of the soft-bodied robot's body, it can be applied not only to the worm robot but also to other forms of soft-bodied robots. For example, when using this method, when a controller learns the behavior of a soft-bodied robot by a method such as reinforcement learning, the robot can be continuously moved without battery replacement. This method is optimal when it is necessary to keep the robot moving continuously without time limitation in the real environment because it is difficult to reproduce and predict the behavior in simulation. Moreover, this method is also useful when a researcher wants to embed several sensor devices and actuators in/on the experimental animal body and feed power to them instead of a soft-bodied robot.

The device here developed represents a robotic platform that can be enhanced with sensor payload. The sensed parameter could, for example, be modulated on the back-coupled signal from the receiver coils, as is the case in near field communication. The inclusion of a payload will bring challenges in the presence of strong magnetic fields needed to actuate the SMAs. Therefore, careful design in terms of shielding and protection of payload elements would be required.

Acknowledgments

The authors would like to acknowledge the members of ERATO Kawahara Project in the University of Tokyo for their feedback. The author (T.U.) also would like to thank Prof. Barry A. Trimmer for his valuable comments and discussion with him and the laboratory member at the Tufts University.

Author Disclosure Statement

No competing financial interests exist.

Funding Information

This work was supported by JST ERATO grant no. JPMJER1501, Japan, and KAKENHI Grant-in-Aid for Scientific Research on Innovative Areas ''Science of Soft Robot'' project funded by JSPS under grant no. 18H05467. In addition, this work was funded by the EU ERASMUS Mundus TEAM Exchange program.

References

1. Kim S, Laschi C, Trimmer B. Soft robotics: a bioinspired evolution in robotics. Trends Biotechnol 2013;31:287–294.
2. Trivedi D, Rahn C, Kier W, *et al.* Soft robotics: biological inspiration, state of the art, and future research. Appl Bionics Biomech 2008;5:99–117.
3. Pfeifer R, Lungarella M, Iida F. The challenges ahead for bio-inspired ''soft'' robotics. Commun ACM 2012;55:76.
4. Pfeifer R, Iida F, Gómez G. Morphological computation for adaptive behavior and cognition. Int Congr Ser 2006;1291: 22–29.
5. Kim B, Lee MG, Lee YP, *et al.* An earthworm-like micro robot using shape memory alloy actuator. Sens Actuators A Phys 2006;125:429–437.
6. Bar-Cohen Y. Artificial muscles using electroactive polymers (EAP): capabilities, challenges and potential. Pasadena, CA: NASA, 2005.
7. Haines CS, Lima MD, Li N, et al. Artificial muscles from fishing line and sewing thread. Science 2014;343:868–872.
8. Shinohara N. Power without wires. IEEE Microw Mag 2011;12:S64–S73.
9. Tesla N. The transmission of electrical energy without wires. Electr World Eng 1904; XLIII:429–431.
10. Covic GA, Boys JT. Inductive power transfer. Proc IEEE 2013;101:1276–1289.
11. Kurs A, Karalis A, Moffatt R, *et al.* Wireless power transfer via strongly coupled magnetic resonances. Science (New York, NY) 2007;317:83–86.
12. Hui SYR, Wenxing Z, Lee CK. A critical review of recent progress in mid-range wireless power transfer. IEEE Trans Power Electron 2014;29:4500–4511.
13. Huh J, Lee SW, Lee WY, *et al.* Narrow-width inductive power transfer system for online electrical vehicles. IEEE Trans Power Electron 2011;26:3666–3679.
14. Sallan J, Villa Gazulla JL, Llombart A, *et al.* Optimal design of ICPT systems applied to electric vehicle

battery charge. IEEE Trans Ind Electron 2009;56:2140–2149.
15. Hui SY. Planar wireless charging technology for portable electronic products and Qi. Proc IEEE 2013;101:1290–1301.
16. Bocan KN, Sejdić E. Adaptive transcutaneous power transfer to implantable devices: a state of the art review. Sensors (Switzerland) 2016;16:E393.
17. Deyle T, Reynolds M. Surface based wireless power transmission and bidirectional communication for autonomous robot swarms. In: Robotics and Automation, ICRA 2008. IEEE International Conference on, 2008, pp. 1036–1041. DOI:10.1109/ROBOT.2008.4543341.
18. Karpelson M, Waters B, Goldberg B, *et al.* A wirelessly powered, biologically inspired ambulatory microrobot. In: Proceedings—IEEE International Conference on Robotics and Automation, 2014, pp. 2384–2391.
19. Zhu K, Nii H, Fernando ONN, *et al.* Selective inductive powering in hardware-based paper computing. In: Lecture Notes in Computer Science (Including Subseries Lecture Notes in Artificial Intelligence and Lecture Notes in Bioinformatics), 2011, pp. 340–344.
20. Boyvat M, Koh JS, Wood RJ. Addressable wireless actuation for multijoint folding robots and devices. Sci Robot 2017;2:eaan1544.
21. Mohamed Ali MS, Takahata K. Wireless microfluidic control with integrated shape-memory-alloy actuators operated by field frequency modulation. J Micromech Microeng 2011;21:75005.
22. Umedachi T, Vikas V, Trimmer BA. Highly deformable 3-D printed soft robot generating inching and crawling locomotions with variable friction legs. In: IEEE International Conference on Intelligent Robots and Systems, 2013, pp. 4590–4595.
23. Casanova JJ, Low ZN, Lin J, *et al.* Transmitting coil achieving uniform magnetic field distribution for planar wireless power transfer system. In: RWS 2009 IEEE Radio and Wireless Symposium, Proceedings, 2009, pp. 530–533.
24. Curran B, Maaß U, Fotheringham G, *et al.* Modeling and characterization of PCB coils for inductive wireless charging. Wirel Power Transf 2015;2:127–133.
25. Waffenschmidt E. Free positioning for inductive wireless power system. In: 2011 IEEE Energy Conversion Congress and Exposition. IEEE, 2011, pp. 3480–3487.
26. Awai I. Basic characteristics of ''Magnetic resonance'' wireless power transfer system excited by a O ohm power source. IEICE Electron Expr 2013;10:1–13.

Address correspondence to:
Takuya Umedachi
Faculty of Textile Science and Technology
Functional Machinery and Mechanics Building
Rm. 2123-15-1
Shinshu University
Tokida
Ueda City
Nagano 386-8567
Japan

E-mail: umedachi@shinshu-u.ac.jp